Supplementary Experimental Section

Materials

1,3-dioxane (DOX, >98%) was purchased from TCI (Shanghai) Development Co., Ltd. Aluminum trifluoromethanesulfonate ($Al(OTf)_3$, 99.9%) was purchased from Sigma-Aldrich (Shanghai) Trading Co., Ltd. The battery separator (Celgard 3501) was purchased from Celgard, LLC. Acetylene black was purchased from Denka Co., Ltd. Lithium bis(fluorosulfonyl)imide (LiFSI) was provided by Guangzhou Tinci Materials Technology Co., Ltd. $LiNi_{0.8}Co_{0.1}Mn_{0.1}O_2$ (NCM811) powder was kindly provided by XTC New Energy Materials (Xiamen) Co., Ltd. Li foil (~400 μm thick), Li_2CoO_2 (LCO) powder, $LiNi_{0.33}Co_{0.33}Mn_{0.33}O_2$ (NCM111) powder, 1,3-dioxolane (DOL, 99.95%), poly(vinylidene fluoride) (PVDF, Mw: 900,000 g mol^{-1}), N-methyl-2-pyrrolidone (NMP, >99.9%), Al current collector, and CR 2032-type coin-cell cases were purchased from Guangdong Canrd New Energy Technology Co., Ltd.

Density functional theory calculation

The molecular geometry and binding energy between one repeating unit of the polymer and one Li^+ was optimized and calculated by density-functional theory (DFT), which was performed using the Gaussian 16 package at the B3LYP/6-311+G(d,p) level.[1] The binding energy (E_B) between Li^+ and the repeating unit was defined as follows:

$$E_B = E_{Li^+-repeating\ unit} - \left(E_{Li^+} + E_{repeating\ unit}\right)$$

where $E_{Li^+-repeating\ unit}$ is the total energy of Li^+ with one repeating unit of the polymer, E_{Li^+} is the energy of a free Li^+, $E_{repeating\ unit}$ is the energy of one repeating unit of the polymer.

The HOMO and LUMO energies of the polymers were also calculated using the Gaussian 16 package at the B3LYP/6-311+G(d,p) level.

Calculation of ionic conductivity, activation energy and Li^+ transference number

The ionic conductivity of the electrolyte was measured using an electrolytic cell with two Pt plates as electrodes via EIS method. The EIS spectra were tested at the

frequency range of 0.1−10^6 Hz with an amplitude of 10 mV at the open-circuit potential. The ionic conductivity (σ) of the electrolyte was calculated by equation (1):

$$\sigma = \frac{k}{R} \qquad \text{* MERGEFORMAT (1)}$$

where R is the bulk resistance of the electrolyte; k is the cell constant calibrated with a standard KCl solution.

The activation energy of Li^+ transport was calculated by equation (2):

$$\sigma = Ae^{\frac{-E_a}{RT}} \qquad \text{* MERGEFORMAT (2)}$$

where A is the pre-exponential factor, E_a is the activation energy of Li^+ transport, R is the ideal gas constant, and T is the testing temperature.

The Li^+ transference number (t_{Li^+}) was estimated according to the AC impedance and direct-current (DC) polarization (with a polarization voltage of 10 mV) using a Li||Li symmetric cell, which was calculated by equation (3):

$$t_{Li^+} = \frac{I_s\left(\Delta V - I_o R_o\right)}{I_o\left(\Delta V - I_s R_s\right)} \qquad \text{* MERGEFORMAT (3)}$$

where I_o and I_s are the initial and steady state current, respectively, R_o and R_s are the initial and steady state resistance, respectively. The EIS spectra were tested at the frequency range of 0.1−10^6 Hz with an amplitude of 10 mV at the open-circuit potential.

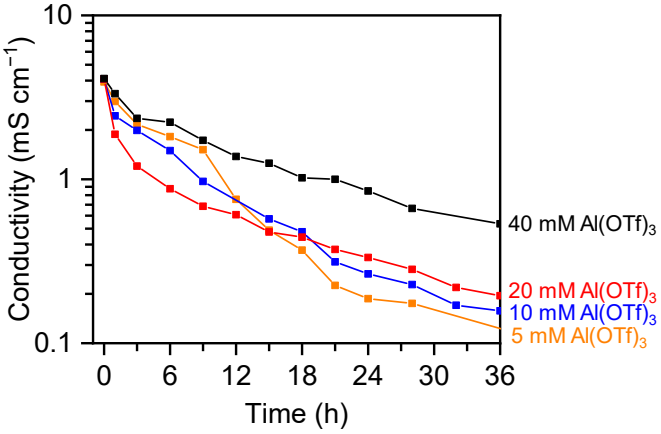

Figure S1. D.C. conductivity versus polymerization time for the P-DOX PE with different amount of $Al(OTf)_3$ initiator.

As shown in the **Figure S1**, after 36 h of the polymerization, the ionic conductivity of the P-DOX PE increases gradually with the increasing amount of $Al(OTf)_3$. However, when the $Al(OTf)_3$ amount was increased to 40 mM, the resulting P-DOX PE was not completely solidified and still has certain fluidity, which may be ascribed to the fact that high initiator concentration would generate abundant initiation center, leading to a low molecular weight of the resulting polymer. Therefore, the amount of $Al(OTf)_3$ was optimized at 20 mM in our study with a balance of ionic conductivity and mechanical strength of the resulting PE.

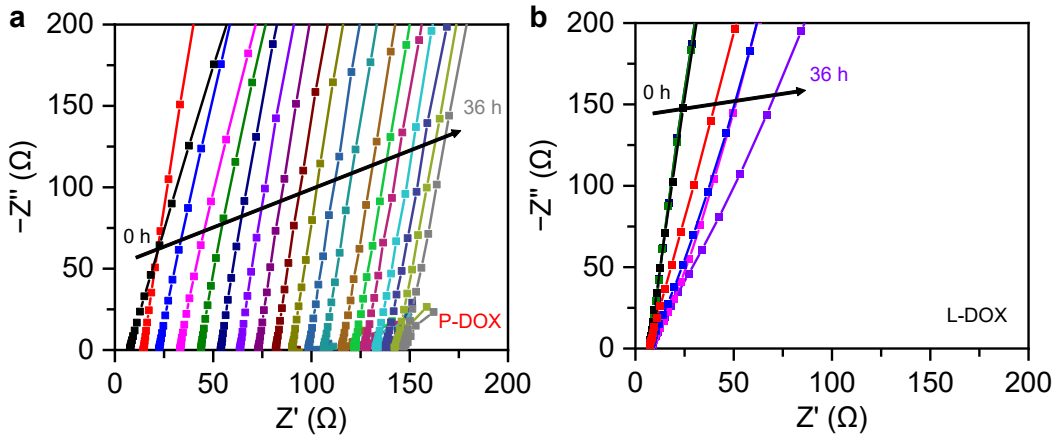

Figure S2. EIS spectra of the Pt||Pt electrolytic cells filled with the L-DOX liquid electrolyte (1.47 m LiFSI/DOX) (a) with and (b) without 20 mM $Al(OTf)_3$ salt after different heating time at 25°C.

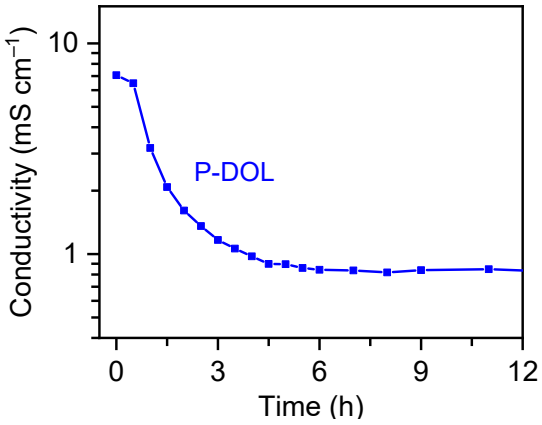

Figure S3. D.C. conductivity versus polymerization time for the P-DOL PE.

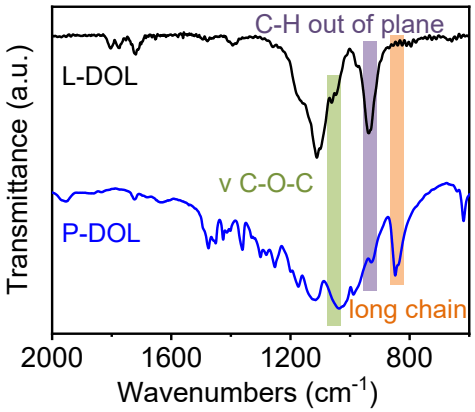

Figure S4. FTIR spectra of the L-DOL liquid electrolyte and P-DOL PE.

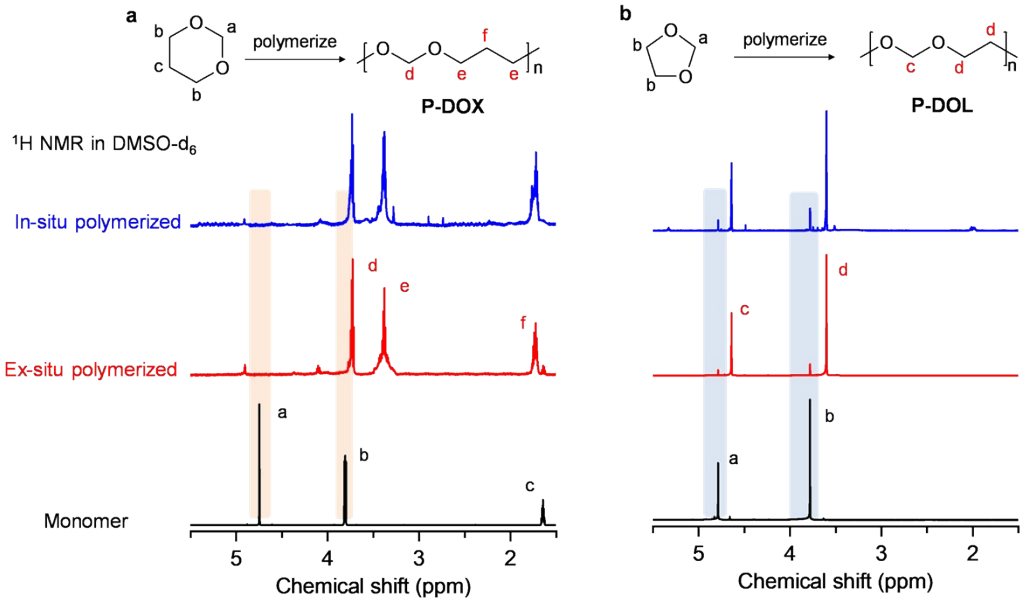

Figure S5. ^{1}H NMR spectra of (a) DOX, ex-situ polymerized P-DOX, and in-situ polymerized P-DOX, and (b) DOL, ex-situ polymerized P-DOL, and in-situ polymerized P-DOL.

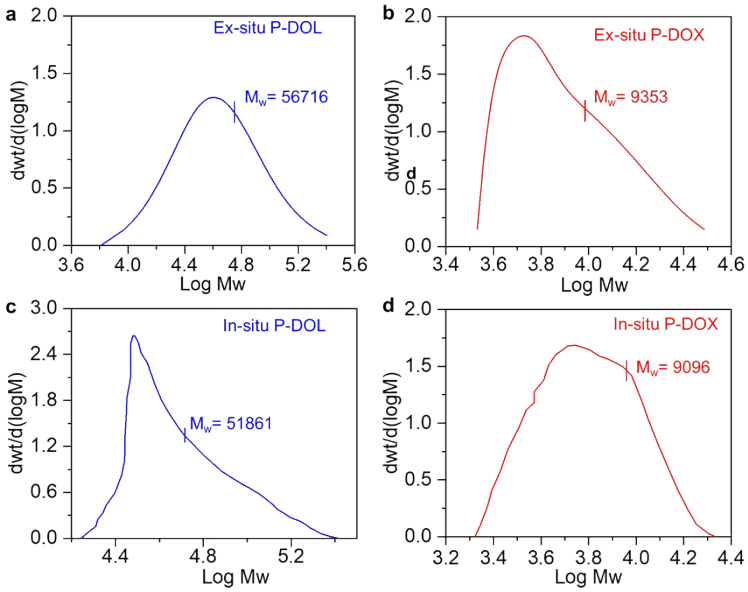

Figure S6. The GPC analysis of (a) ex-situ polymerized P-DOL, (b) ex-situ polymerized P-DOX, (c) in-situ polymerized P-DOL, and (d) in-situ polymerized P-DOX.

Table S1. Detailed GPC analysis of P-DOL and P-DOX PEs.

	M_n	M_w	M_P	M_z	M_{z+1}	M_z/M_w
ex-situ P-DOL	33950	56716	47222	97917	159155	1.7264
ex-situ P-DOX	7053	9353	4944	13062	17645	1.3965
in-situ P-DOL	41141	51861	30148	74258	109544	1.2606
in-situ P-DOX	7532	9096	5434	10596	11827	1.2077

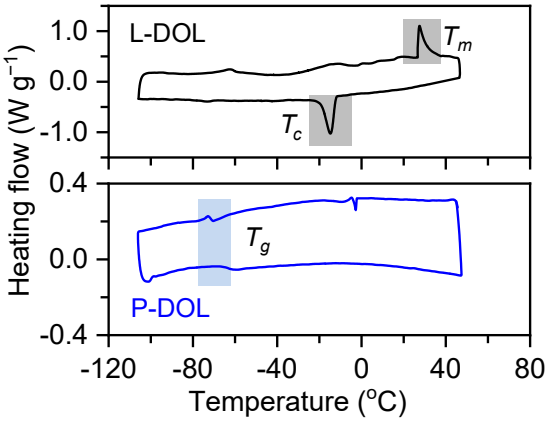

Figure S7. DSC curves of L-DOL liquid electrolyte (top) and P-DOL PE (bottom), of which the shaded areas indicate the melting peak (T_m), crystallization peak (T_c), and glass transition peak (T_g) respectively.

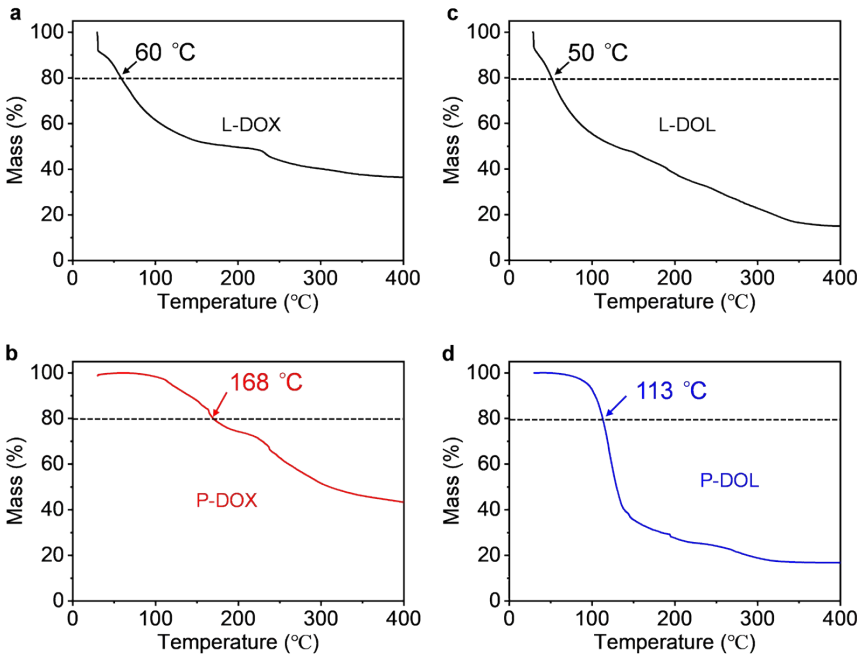

Figure S8. TGA profiles of (a) L-DOX, (b) P-DOX, (c) L-DOL, and (d) P-DOL. The decomposition temperature, corresponding to 20% weight lost, was marked.

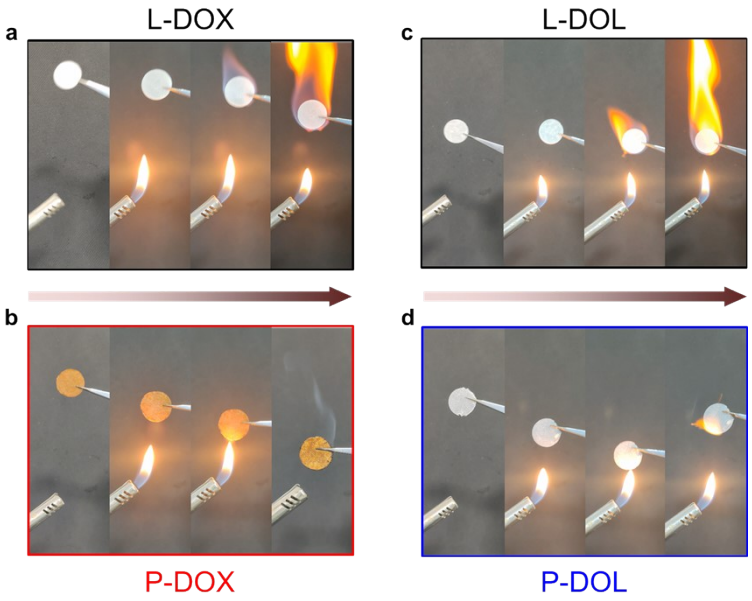

Figure S9. Flammability tests of the glass fiber separators infiltrated with (a) L-DOX, (b) P-DOX, (c) L-DOL, and (d) P-DOL electrolytes.

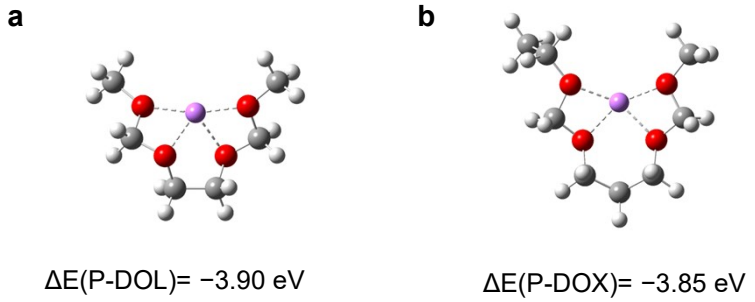

Figure S10. Binding energies (E_B) between Li^+ and (a) P-DOL repeat unit and (b) P-DOX repeat unit.

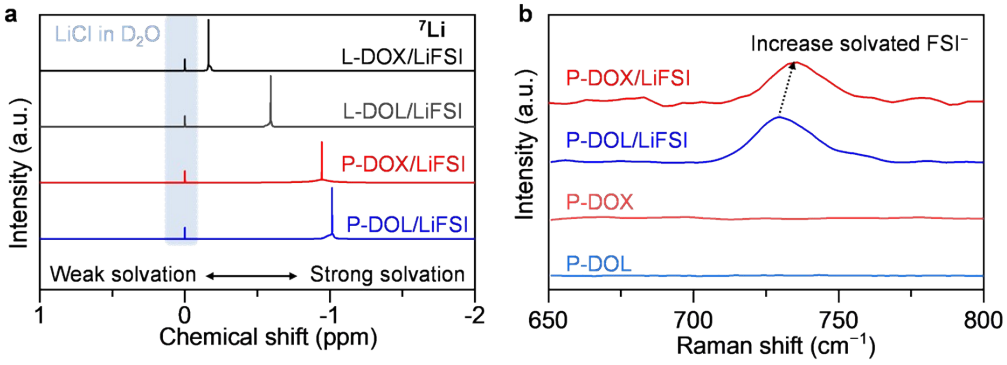

Figure S11. (a) ^{7}Li NMR for various electrolytes. The chemical shifts of all samples were calibrated using 10 mM LiCl in D_2O at 0 ppm. (b) Raman spectra of the polymer electrolytes and their corresponding polymers.

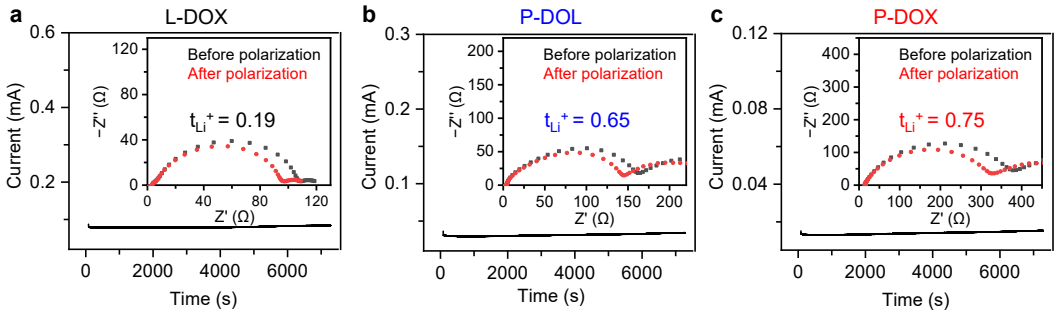

Figure S12. Li^+ transference numbers of (a) L-DOX, (b) P-DOL, and (c) P-DOX electrolytes.

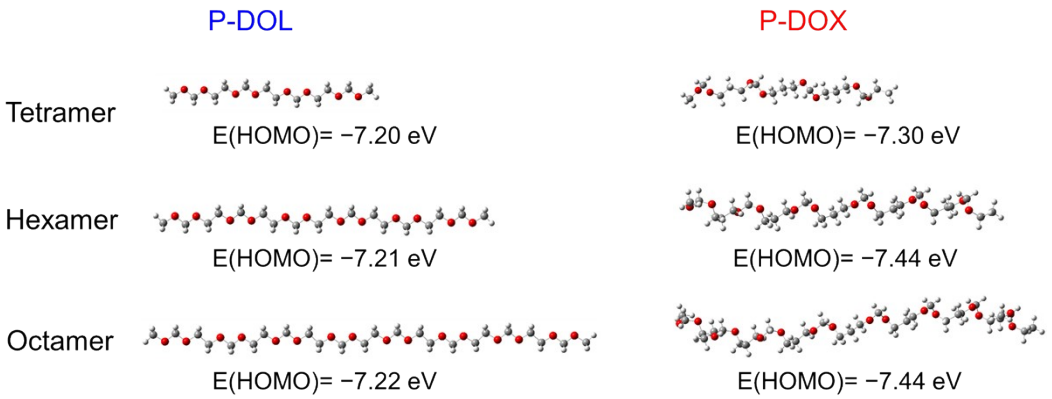

Figure S13. The HOMO energies of P-DOL and P-DOX polymers with different chain length.

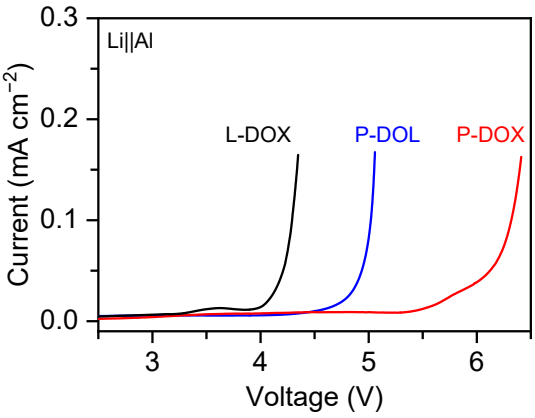

Figure S14. LSV of the electrolytes at a scan rate of 1 mV s^{-1} with Al foil as working electrode.

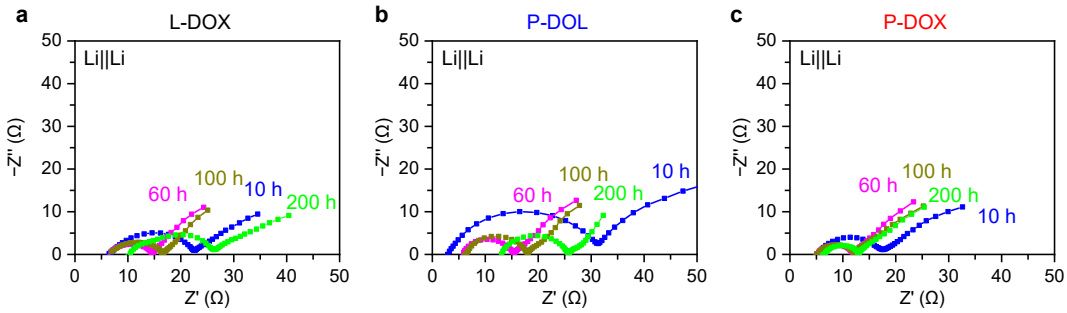

Figure S15. EIS spectra of the Li||Li symmetric cells using (a) L-DOX, (b) P-DOL, and (c) P-DOX electrolytes after different plating/stripping cycles at a current density of 1.0 mA cm^{-2} with a capacity of 1.0 mAh cm^{-2}.

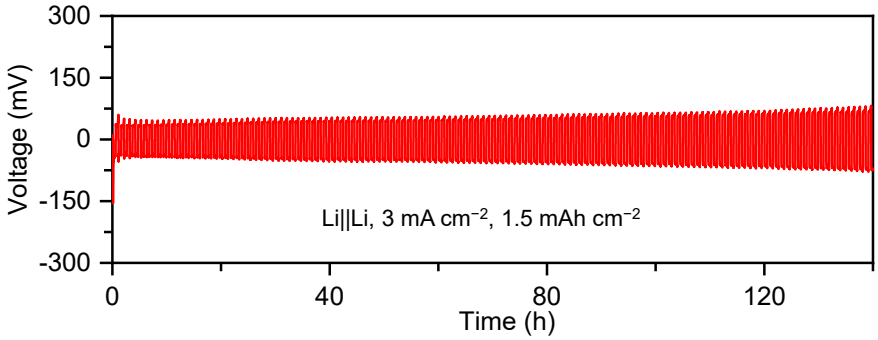

Figure S16. Long-term cycling of Li||Li symmetrical cells using P-DOX PE at a current density of 3.0 mA cm^{-2} with a capacity of 1.5 mAh cm^{-2}.

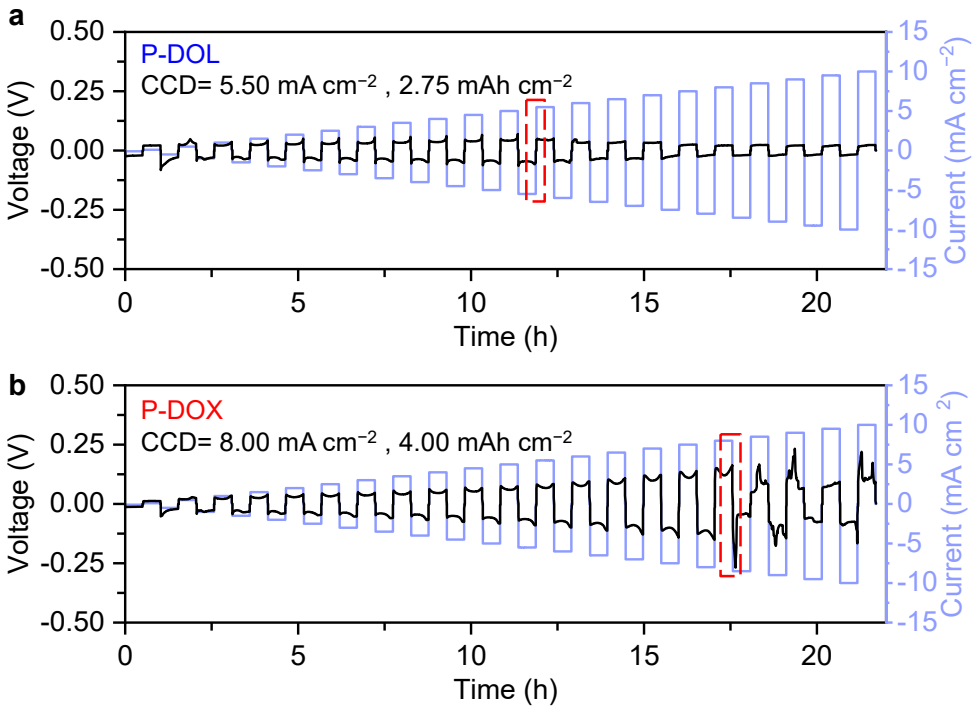

Figure S17. Critical current density tests of Li||Li symmetric cell using (a) P-DOL and (b) P-DOX PEs.

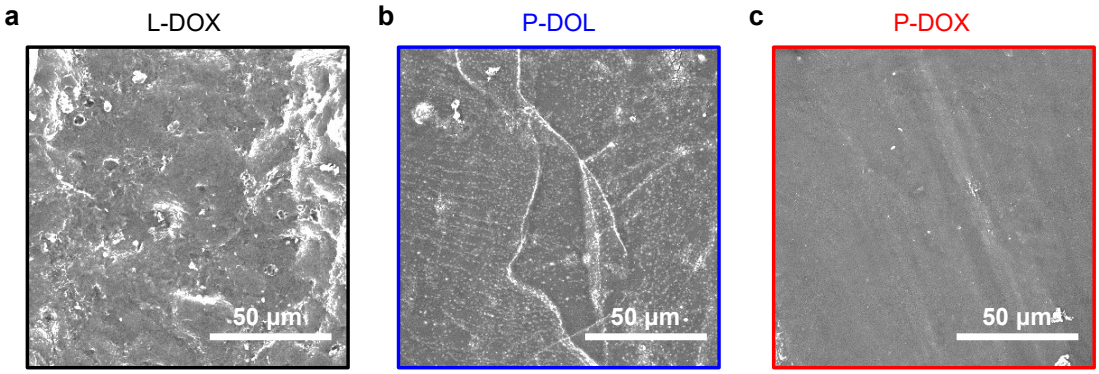

Figure S18. SEM images of Li-metal electrode in Li||Li cells using (a) L-DOX, (b) P-DOL, and (c) P-DOX electrolytes after 200 plating/stripping cycles at a current density of 1.0 mA cm^{-2} with a capacity of 1.0 mAh cm^{-2}.

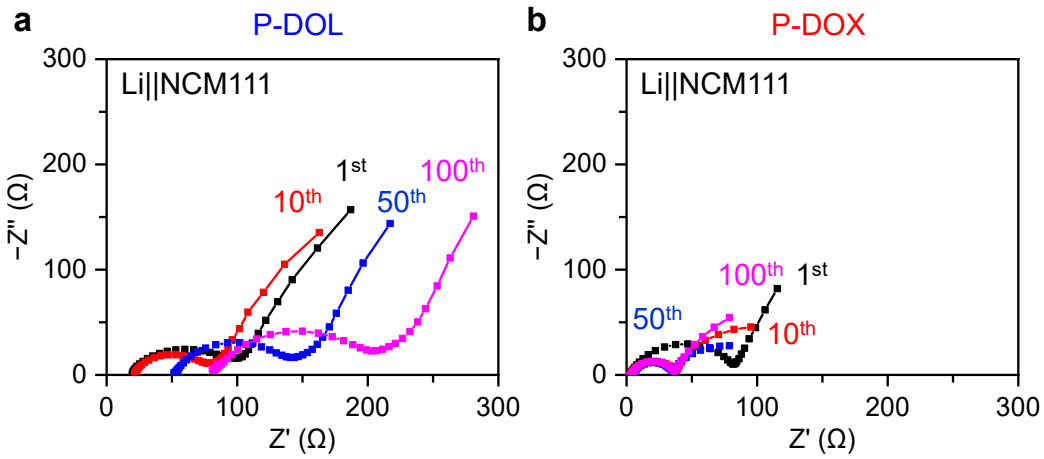

Figure S19. EIS spectra of Li||NCM111 cells using (a) P-DOL and (b) P-DOX electrolytes after different cycles at a current density of 0.5 C.

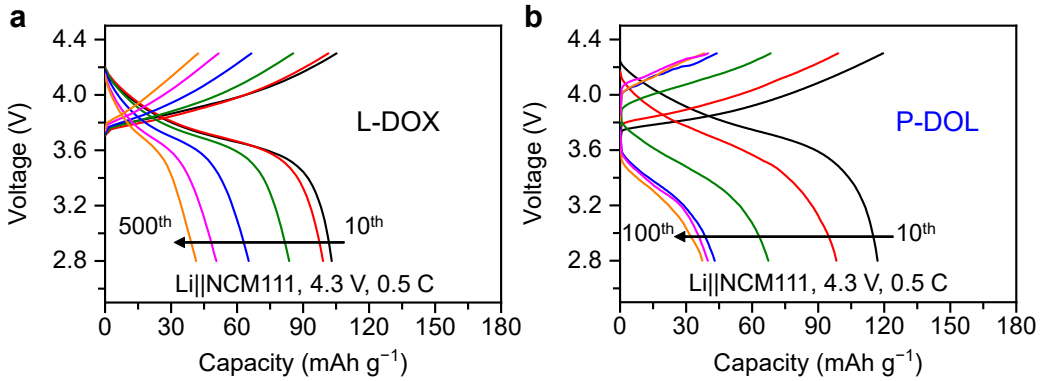

Figure S20. Selected charge-discharge profiles of Li||NCM111 cells using (a) L-DOX and (b) P-DOL electrolytes within a cutoff voltage of 2.8-4.3 V at 0.5 C.

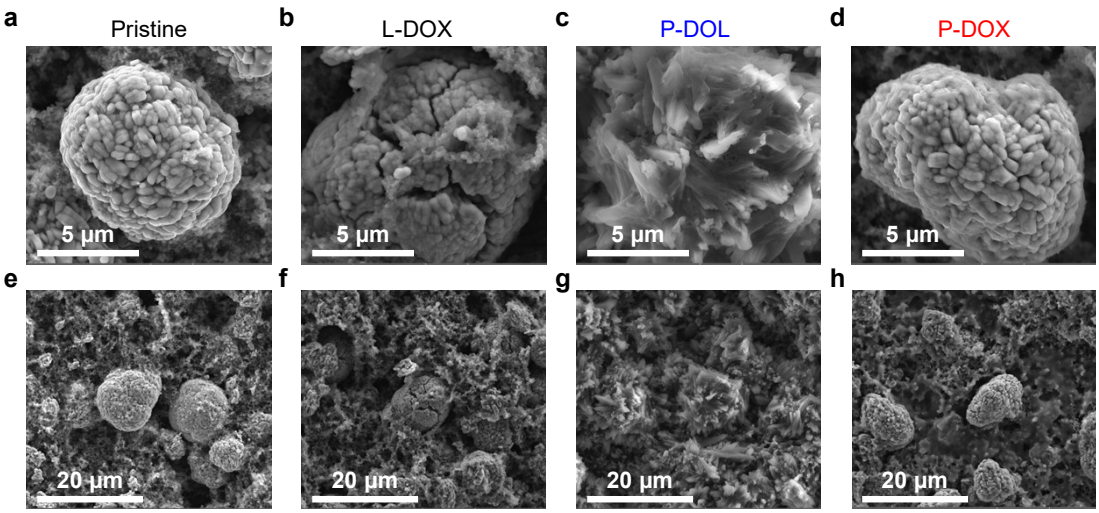

Figure S21. SEM image of the NCM111 cathodes (a, e) before cycling and after 500 cycles in Li||NCM111 cells using (b, f) L-DOX, (c, g) P-DOL, and (d, h) P-DOX electrolytes.

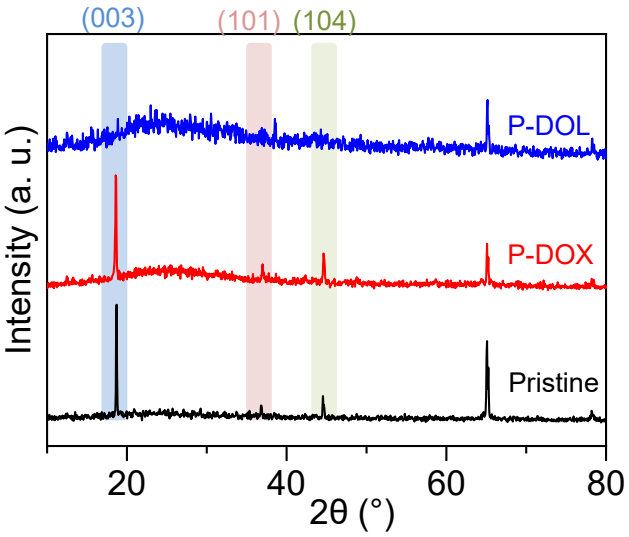

Figure S22. The XRD patterns of the NCM111 cathode before and after 500 cycles in Li||NCM111 cells using P-DOL and P-DOX PEs at 0.5 C.

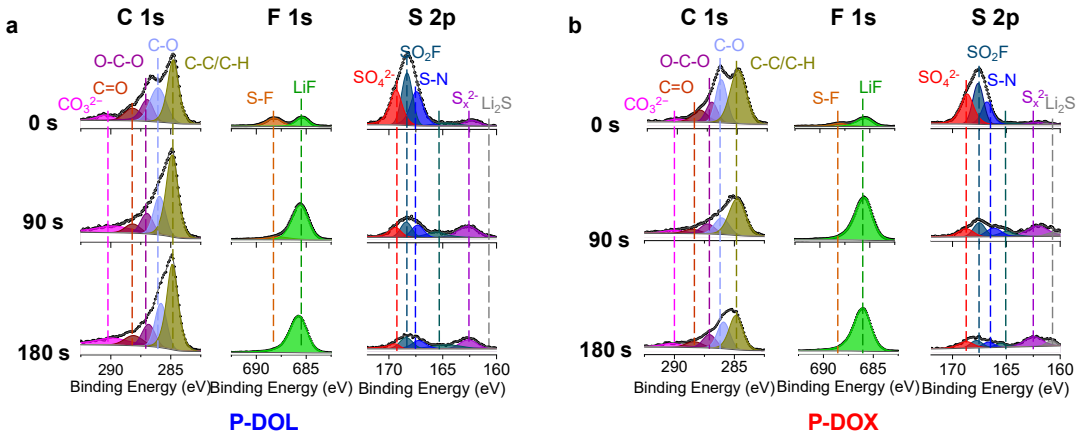

Figure S23. Characterization of the surface components on NCM111 cathode. XPS depth profiles of the NCM111 cathodes after 500 cycles in Li||NCM111 cells using (a) P-DOL and (b) P-DOX PEs at 0.5 C.

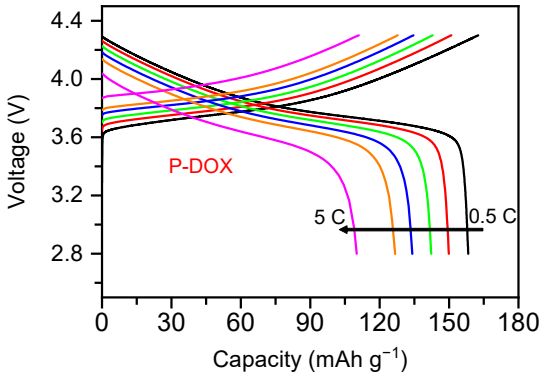

Figure S24. Selected charge-discharge profiles of the Li||NCM111 cell using P-DOX PE at different rates.

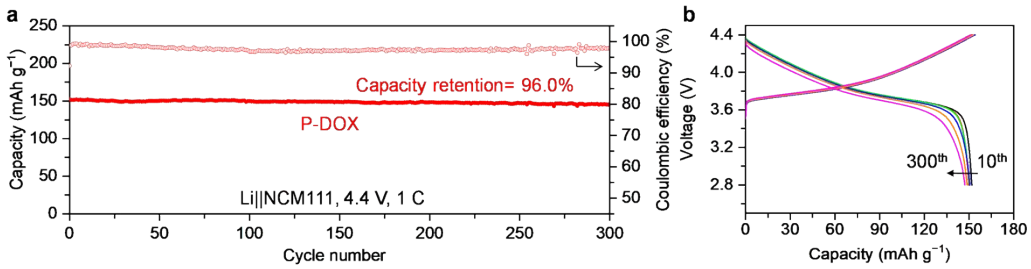

Figure S25. (a) Cycling performance and (b) selected charge-discharge profiles of the Li||NCM111 full-cell using P-DOX PE within a cutoff voltage of 2.8-4.4 V at 1.0 C.

Table S2. The comparisons of this work with state-of-the-art reported in-situ polyether-based electrolytes for high-voltage LMBs.[2-14]

Monomer	Solvent/ additives	Cathode	Cut-off voltage (V)	Rate (C)	Initial capacity (mAh g^{-1})	Cycles	Capacity retention (%)	Ref
DOX	——	NCM11	4.3	0.5	153.2	500	95.5	This work
			4.4	1	151.6	300	96.0	
			4.5	1	154.3	100	96.0	
		NCM811	4.5	1	195.3	100	84.0	
		LCO	4.5	1	163.6	100	92.9	
DOL	——	NCM622	4.3	0.5	167.3	200	78.9	[2]
DOL	——	NCM622	4.2	0.1	152.9	60	78.5	[3]
DOL	EC/DEC/DMC(50%)	NCM622	4.3	0.2	173.9	200	82.8	[4]
		NCM811	4.3	0.2	188.9	120	83.1	
DOL	EC/DEC/DMC(50%) +TPP	NCM622	4.3	0.5	150	100	93	[5]
		NCM811	/	0.5	188	100	78	
DOL	N1222FSI	NCM622	4.3	0.2	153.7	100	81.3	[6]
DOL	DME(25%) +MSP/KMSP separator	NCM811	4.4	1	179.7	500	80.2	[7]
DOL	FEC(40%)+ HDI	LCO	4.2	0.5	131	500	80	[8]
DOL	SN(25%)+FEC(5%) +PVDF-HFP	NCM811	4.3	1	141.6	100	70.6	[9]
DOL	——	NCM622	4.3	0.1	155	5	/	[10]
DOL	DME (50%)	NCM622	4.3	0.1	164.1	100	90.6	[11]
DOL	MP (60%) +FEC	NCM811	4.3	1	169	200	82	[12]
DOL	SN (30%)	LMO	4.3	0.1	98.7	126	92.5	[13]
		LCO	4.3	0.1	131(313 K)	60	61	
DOL	EC (37%)	NCM811	4.3	0.2/ 0.4	186.6	150	74.5	[14]
				0.32	177.4	50	96.4	

Note: the cells were tested at room temperature unless otherwise stated.

Supporting References

1. M. J. Frisch, G. W. Trucks, H. B. Schlegel, G. E. Scuseria, M. A. Robb, J. R. Cheeseman, G. Scalmani, V. Barone, G. A. Petersson, H. Nakatsuji, X. Li, M. Caricato, A. V. Marenich, J. Bloino, B. G. Janesko, R. Gomperts, B. Mennucci, H. P. Hratchian, J. V. Ortiz, A. F. Izmaylov, J. L. Sonnenberg, Williams, F. Ding, F. Lipparini, F. Egidi, J. Goings, B. Peng, A. Petrone, T. Henderson, D. Ranasinghe, V. G. Zakrzewski, J. Gao, N. Rega, G. Zheng, W. Liang, M. Hada, M. Ehara, K. Toyota, R. Fukuda, J. Hasegawa, M. Ishida, T. Nakajima, Y. Honda, O. Kitao, H. Nakai, T. Vreven, K. Throssell, J. A. Montgomery Jr., J. E. Peralta, F. Ogliaro, M. J. Bearpark, J. J. Heyd, E. N. Brothers, K. N. Kudin, V. N. Staroverov, T. A. Keith, R. Kobayashi, J. Normand, K. Raghavachari, A. P. Rendell, J. C. Burant, S. S. Iyengar, J. Tomasi, M. Cossi, J. M. Millam, M. Klene, C. Adamo, R. Cammi, J. W. Ochterski, R. L. Martin, K. Morokuma, O. Farkas, J. B. Foresman and D. J. Fox, *Gaussian 16 Rev. A.03*, 2016.
2. J. Xiang, Y. Zhang, B. Zhang, L. Yuan, X. Liu, Z. Cheng, Y. Yang, X. Zhang, Z. Li, Y. Shen, J. Jiang and Y. Huang, *Energy & Environmental Science*, 2021, **14**, 3510-3521.
3. C. Z. Zhao, Q. Zhao, X. Liu, J. Zheng, S. Stalin, Q. Zhang and L. A. Archer, *Adv Mater*, 2020, **32**, e1905629.
4. J. Y. Liang, X. D. Zhang, Y. Zhang, L. B. Huang, M. Yan, Z. Z. Shen, R. Wen, J. Tang, F. Wang, J. L. Shi, L. J. Wan and Y. G. Guo, *J Am Chem Soc*, 2021, **143**, 16768-16776.
5. Q. Ma, J. Yue, M. Fan, S. J. Tan, J. Zhang, W. P. Wang, Y. Liu, Y. F. Tian, Q. Xu, Y. X. Yin, Y. You, A. Luo, S. Xin, X. W. Wu and Y. G. Guo, *Angew Chem Int Ed Engl*, 2021, **60**, 16554-16560.
6. A. Hu, Z. Liao, J. Huang, Y. Zhang, Q. Yang, Z. Zhang, L. Yang and S.-i. Hirano, *Chemical Engineering Journal*, 2022, **448**.
7. D. Chen, T. Zhu, M. Zhu, S. Yuan, P. Kang, W. Cui, J. Lan, X. Yang and G. Sui, *Energy Storage Materials*, 2022, **53**, 937-945.
8. Z. Geng, Y. Huang, G. Sun, R. Chen, W. Cao, J. Zheng and H. Li, *Nano Energy*, 2022, **91**.
9. Y. Liu and Y. Xu, *Chemical Engineering Journal*, 2022, **433**, 137661.
10. Q. Zhao, X. Liu, S. Stalin, K. Khan and L. A. Archer, *Nature Energy*, 2019, **4**, 365-373.
11. F. Q. Liu, W. P. Wang, Y. X. Yin, S. F. Zhang, J. L. Shi, L. Wang, X. D. Zhang, Y. Zheng, J. J. Zhou, L. Li and Y. G. Guo, *Sci Adv*, 2018, **4**, eaat5383.
12. J. Yu, X. Lin, J. Liu, J. T. T. Yu, M. J. Robson, G. Zhou, H. M. Law, H. Wang, B. Z. Tang and F. Ciucci, *Advanced Energy Materials*, 2021, **12**, 2102932.
13. Q. Liu, B. Cai, S. Li, Q. Yu, F. Lv, F. Kang, Q. Wang and B. Li, *Journal of Materials Chemistry A*, 2020, **8**, 7197-7204.
14. Q. Zhao, X. Liu, S. Stalin and L. Archer, *Cell Reports Physical Science*, 2020, **1**, 100146.